

# Analog Pulse Shape Discrimination Circuit for High Event Rates and Fast Scintillators with a Dynamic Deadtime

Itai Morad<sup>1\*</sup>, Max Ghelman<sup>2</sup>, Alon Osovizky<sup>2,3</sup>, Amir Ellenbogen<sup>2</sup>, Rami Seif<sup>2</sup>, Eran Vax<sup>2</sup>, Amir Broide<sup>2</sup>, and Ron Harn<sup>2</sup>

<sup>1</sup>Israel Atomic Energy Commission (IAEC),

<sup>2</sup>Nuclear Research Center Negev (NRCN),

<sup>3</sup>Radiation Detection Department, Rotem Industries Ltd

(\*) itaimorad1111@gmail.com

**Abstract**—We developed an analog pulse shape discrimination (PSD) topology based on the well-established charge integration (CI) method, featuring two novel functional blocks beneficial for high event rate operation. The topology is designed for high-speed scintillators. The demonstrated analog design is potentially better suited than digital methods, when considering both processing time and power consumption aspects. The topology was tested using both experimental alpha and beta pulses from a plastic scintillator with a layer of ZnS(Ag) coupled to a PMT, and a fast digital emulator to simulate controlled high event rate scenarios. The discrimination capabilities of the topology were optimized and evaluated using a traditional figure of merit (FoM) approach. The topology achieved over 99% correct classifications when evaluated using the experimental pulses recorded. Additionally, the dedicated blocks resulted in a fourfold reduction in miss-classifications of slow pulses at an event rate of 100 kcps of fast pulses, while also providing a dynamic deadtime proportional to the pulse charge.

**Keywords**—pulse shape discrimination, high rate, charge integration, analog circuit, plastic scintillator.

## I. INTRODUCTION

THE term PSD is a general name for techniques used to discriminate between different types of radiation based on differences between the nuclear pulse shapes. PSD can be applied to detectors of ionizing radiation with the ability to interact with multiple kinds of radiation. It is often important to distinguish different types of radiation for homeland security, nuclear safeguard, and neutron scattering applications [1]–[4]. PSD can either be performed directly on the detector signal in the analog domain, or on the sampled detector signal in the digital domain. PSD methods realized in the analog and digital domain vary in their discrimination capabilities and power consumption. Traditional digital signal processing algorithms include slice-fitting, tail-sum, cosine similarity, histogram-difference, and Fourier analysis based methods [3]–[10]. In addition, recent advancements in the field of artificial intelligence have given rise to PSD techniques based on traditional machine learning [11]–[14] and neural networks [2], [15]–[20]. Digital PSD methods require high-speed analog to digital converters (ADCs) which increases power consumption. In addition, some of these algorithms are complex and require long processing times, resulting in a limited count rate and increasing deadtime. Performing PSD in the analog domain

may be more suitable for applications with limited hardware that require low power consumption. This is particularly true when working with fast decay scintillators, especially for battery-based applications.

Discrimination capabilities of PSD techniques applied in the analog domain are limited to what is achievable with integrated circuits (ICs). Pulse height discrimination (PHD) techniques discriminate the pulses based on amplitude or charge [21], while pulse width discrimination (PWD) techniques such as time over threshold (ToT) discriminate the pulses based on their duration [22]. Such techniques are often simple to realize and suffer from a considerable number of miss-classifications in low signal-to-noise ratio (SNR). In addition, operation within high event rates may cause an additional number of miss-classifications due to pileup.

In this work, a novel analog PSD topology for fast scintillators is presented. Discrimination is based on the well-established digital CI method, providing superior discrimination capabilities compared to analog methods based on PHD and PWD. The topology introduces two dedicated blocks designed to improve neutron count rate when operating within high event rates. The double<sup>+</sup> counting rejection (D<sup>+</sup>CR) block was designed to reject gammas arriving consecutively, resulting in fewer neutron miss-classifications in high gamma fluxes. Moreover, the dynamic deadtime (DDT) block was designed to produce a deadtime proportional to the energy of the pulse, lowering the total deadtime and improving detection efficiency.

Alpha and beta pulses interacting with a plastic and ZnS(Ag) scintillator coupled to a photomultiplier tube (PMT) were recorded and analyzed in order to design the analog topology. The topology was implemented on an FR-4 printed circuit board (PCB) designed for high frequency operation. Experiments with both radioactive sources and a fast digital emulator were carried out in order to assess the discrimination capabilities of the method. Results show excellent discrimination capabilities and successfully validate the contribution of the D<sup>+</sup>CR block and the DDT block in high event rate scenarios.

The rest of this article is organized as follows. The experimental setup, data analysis, and the challenges associated with

performing analog PSD for fast scintillators under high event rates are described in section II. section III provides a detailed description of the proposed PSD method. Discrimination capabilities of the proposed method under various conditions are displayed in section IV. Finally, we provide a summary and discuss some future possibilities in section V.

## II. DATA

### A. Experimental Setup and Data Analysis

The experimental setup used is described as follows. Alpha and beta sources were placed in front of a plastic scintillator with a ZnS(Ag) layer. The alpha particles interact with the ZnS(Ag) layer, while the beta particles interact with the plastic. The scintillator was coupled to a PMT. 20,000 alpha and 20,000 beta pulse shapes were recorded using a fast digital oscilloscope. The amplitudes and decay constants of the recorded pulses were digitally fit using non-linear optimization and are scattered in Fig. 1. The amplitudes of both the alpha and beta pulses fall within a similar range; therefore, they cannot be discriminated using PHD methods. The fitted decay constants of beta pulses extend up to around 10 ns, while the fitted decay constants of alpha pulses range between approximately 10 ns and 70 ns, establishing a distinct separation of alpha and beta pulses within the decay constant domain. The variance of the fitted decay constants higher for low energy pulses due to SNR, which results in noisy fitting. Considering these pulse characteristics, the selection of the discrimination method employed in the topology is grounded in the well-established CI method, commonly utilized in the digital domain. Discrimination using the CI method relies significantly on the decay constant parameter, rendering it a suitable choice for our data set.

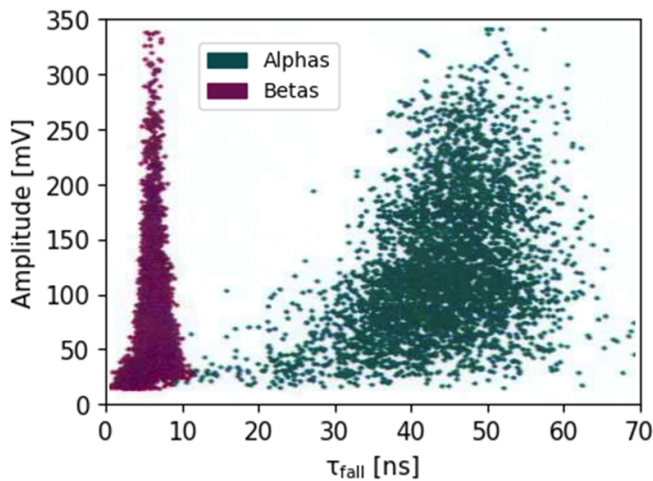


Fig. 1. The distribution of the alpha and beta pulses over the amplitude-decay constant span.

### B. Challenges

Although the CI method is based on simple principles and has been shown to possess excellent PSD capabilities [23], implementing the method in an analog fashion for fast

scintillators while operating in high event rates poses several challenges.

**Challenge I: Fast scintillation responses.** As can be seen in Fig. 1, scintillation responses of beta or gamma particles in plastic scintillators decay within several ns. Processing and discrimination of these responses demand high-speed components and careful analog design. Small timing jitters within the order of ns, and other timing uncertainties like walk or drift, highly affect the processing of these pulses.

**Challenge II: Miss-classifications in high event rates.** Discrimination based on the CI method is based on a ratio between two integral values referred to as the *PSD ratio*. In the case of two beta pulses arrive consecutively, the resulting PSD ratio is prone to resemble the PSD ratio of an alpha pulse, resulting in a miss-classification. This event is more likely to occur in high beta event rates. Applications such as neutron scattering demand accurate neutron counting, while the accuracy constraint for gamma counting is less strict [2]. Therefore, accurately counting neutron arrivals in high gamma fluxes is challenging.

**Challenge III: deadtime in high event rates.** A constant deadtime introduces a trade-off between counting accuracy and detection efficiency. For short deadtimes, long-lasting alpha scintillation responses will re-trigger the system multiple times, resulting in the classification of a single alpha pulse as multiple alpha pulses. For long deadtimes proportional to the length of the longest lasting alpha pulses, which are in the order of  $\mu\text{s}$ , events arriving during the deadtime will be rejected and missed [24].

## III. PROPOSED METHOD

In this section, we introduce our analog PSD topology for fast scintillation responses which is based on the CI method. Discrimination relies on pulse energy, delineating three distinct regions where the most suitable method is applied for discrimination within each. Discrimination features are extracted in the block referred to as the *discrimination block*. The block where the output decision pulses are produced, based on the discrimination features, is referred to as the *decision block*.

As our design is geared towards high rates, two dedicated blocks for **Challenge II** and **Challenge III** are introduced. The  $D^+CR$  block is designed to improve classification accuracy in high rates by detecting and rejecting the event of two beta pulses arriving consecutively, which is prone to be miss-classified as an alpha. The  $DDT$  block is designed to improve detection efficiency by introducing a dynamic deadtime, proportional to the charge of the arriving pulses. Moreover, a varying constant deadtime is introduced in the discrimination block to further improve detection efficiency in high rates. A block diagram of the topology can be viewed in Fig. 2. The nuclear pulse arriving from the PMT is fed into the discrimination block, the  $D^+CR$  block, the  $DDT$  block, and the block referred to as the *control signals block*. The design of the control signals block aims to detect the incoming nuclear pulse and generate digital signals. These digital signals are instrumental in controlling the timing of various processes that take place within the other blocks, and

are therefore fed into the other blocks. The outputs from both the discrimination block and the D<sup>+</sup>CR block are channeled into the decision block due to their direct relevance to the discrimination decision-making process. Next, we elaborate on the discrimination method and the blocks dedicated to improve operation in high rates.

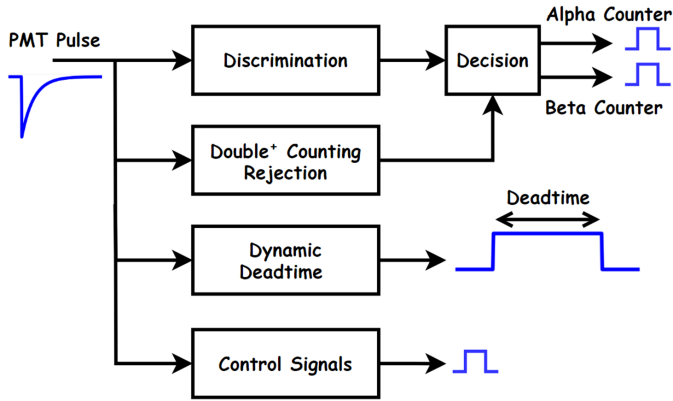


Fig. 2. Block diagram of the proposed method.

### A. Discrimination Method

A scheme of the proposed PSD topology based on the CI method is shown in Fig. 3. The nuclear pulse is amplified and shaped. Then, the pulse is fed into two parallel channels referred to as the *partial channel* and the *full channel*, where the partial channel performs integration to compute  $V_{partial}$  and the full channel performs integration to compute  $V_{full}$ .  $V_{partial}$  and  $V_{full}$  are then fed into three comparators, which combined with logic gates discriminate the nuclear pulse as either an alpha or a beta. Two examples of signal shape at different nodes of the electronic topology for an alpha pulse and a beta pulse can be seen in Fig. 4. The digital signals produced by the control signals block which time the different components can be seen in Fig. 5.

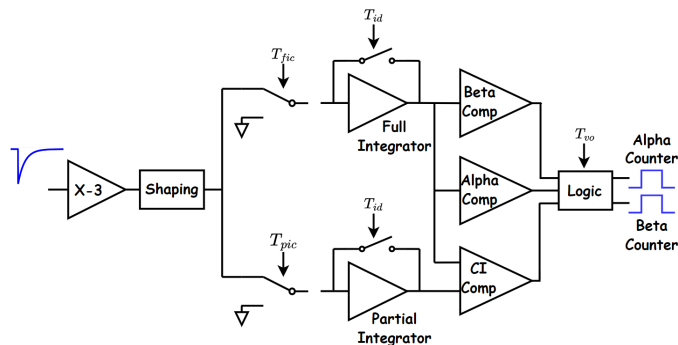


Fig. 3. Illustration of the Discrimination block and alongside the Decision block.

The nuclear pulse is fed from the detector to a high bandwidth amplifier. It is important for the pre-amplifier to have high amplification, the ability to recover from saturation, and large bandwidth. A sufficiently large bandwidth ensures the shape of the pulses is preserved and discrimination capabilities are not harmed. Therefore, the pre-amplifier should

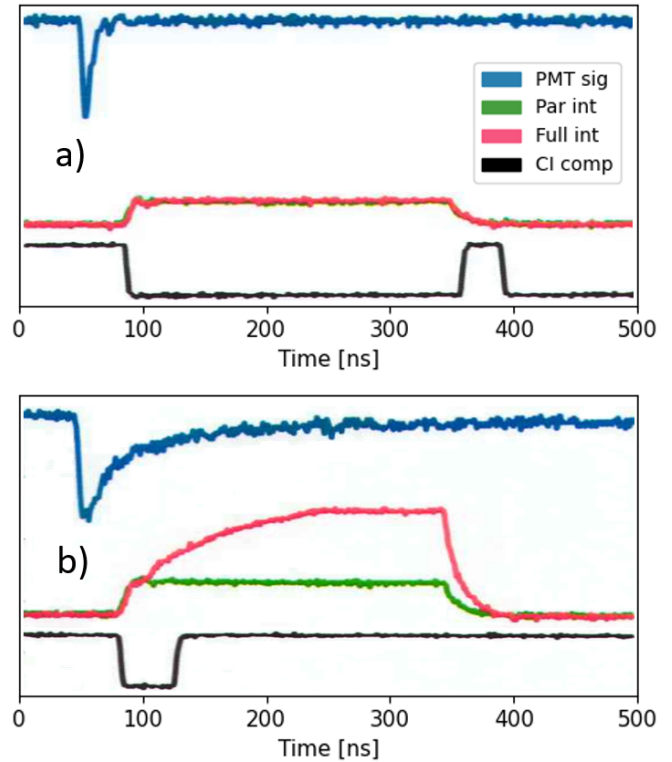


Fig. 4. Signal shape at different nodes of the discrimination block (a) for a beta pulse, (b) for an alpha pulse.

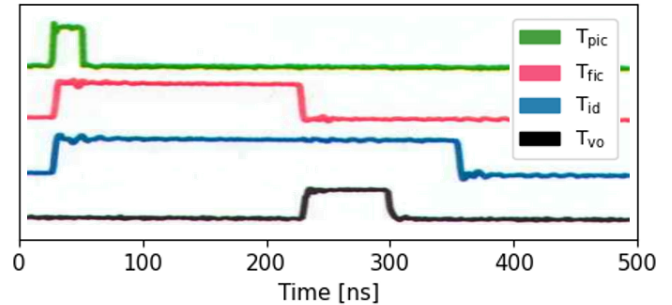


Fig. 5. Signal shape at different nodes of the control signals block. When  $T_{pic}$  is high the pulse is injected into the partial integration channel. When  $T_{fic}$  is high the pulse is injected into the full integration channel. When  $T_{id}$  is low both integrators are discharged. When  $T_{vo}$  is high the decision block is enabled to produce the output pulse.

be carefully selected, by referring to its bandwidth and noise level, compared to the detector's pulse shape and internal noise level. The amplifier output is fed into a detection channel and a classification channel.

The detection channel is responsible for both detection of the pulses and monitoring of various processes within the circuit. Pulse detection is carried out by feeding the amplifier output into a comparator level that generates a digital pulse. The threshold level is set as low as possible such that the detector noise does not cause false alarms. Monitoring of the various processes within the circuit is carried out by feeding the comparator digital signal into a chain of monostable multivibrators, which produce digital signals. Examples of

these signals and their associated roles are depicted in X.Fig. 5. It can be seen that  $T_{pic}$  lasts 25 ns. Due to the lack of monostable multivibrators able to produce such short signals, a custom made topology mimicking the behavior of a monostable multivibrator utilizing a RC network, a comparator, and an AND logic gate was realized.

The classification channel is responsible for classification. First, the amplified pulse is further processed and shaped. Then, it is fed into two channels, a partial integration channel and a full integration channel. Each channel consists of a single pole double throw (SPDT) analog switch responsible for feeding the pulse into the integrator during its respective integration period, and ground otherwise, an integrator, and a single pole single throw (SPST) analog switch responsible for discharging the integrator. There is a time delay introduced from the moment of detection up until the integrators begin integrating the pulse. The time delay is dictated by the propagation delay of the following components:

$$T_{\text{detection comparator}} + T_{\text{monostable multivibrator}} + T_{\text{SPDT switch}} \quad (1)$$

Due to **Challenge I**, by the time the pulse is fed into the integrator, fast scintillation responses that decay within several ns diminish and relevant information for discrimination is lost. To address this issue, the amplified pulse undergoes an additional delay and shaping process, ensuring the preservation of its information. This results in attenuation of the high frequency components, causing beta pulses to look more similar to alpha pulses, which increases the probability of miss-classification. A trade-off between preserving relevant information for discrimination and making alpha and beta pulses more similar is introduced.

The tuples of  $V_{\text{partial}}$ ,  $V_{\text{full}}$  measured for alpha and beta pulses obtained during the experiment described in section II are scattered in Fig. 6. The PSD ratio is computed via (2) and is used for discrimination in the CI region visualized in Fig. 6 as the region where  $0.3 \text{ V} < V_{\text{full}} < 1.7 \text{ V}$ .

$$PSD \text{ ratio} = \frac{V_{\text{full}}}{V_{\text{partial}}} \quad (2)$$

Implementing analog division, which is needed in order to calculate the PSD ratio in (2), often relies on the exponential characteristics of PN-junctions and requires several components. Fortunately, our task doesn't involve calculating the PSD ratio, but rather entails comparing it to a threshold to discriminate between alpha and beta pulses. This comparison can be effectively executed using the CI comparator. In this setup, the (-) input is supplied with  $V_{\text{partial}}$ , while the (+) input receives  $V_{\text{full}}$  after undergoing voltage division to yield  $V_{\text{full}} / THR$ .

However, not all pulses require the CI method. The charge of the pulse is directly proportional to  $V_{\text{full}}$ . As depicted in Fig. 6, it becomes evident that only beta pulses fall within the range of  $V_{\text{full}} < 0.3 \text{ V}$  (to the left of the blue dotted line), and thus, they are automatically discriminated by the Beta comparator without the necessity of the CI method. Similarly, only alpha pulses fall within the range of  $V_{\text{full}} > 1.7 \text{ V}$  (to the right of the red dotted line) and thus, they are automatically

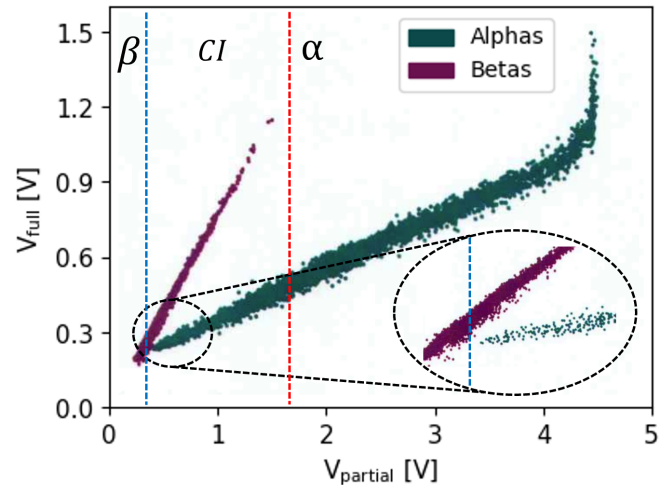


Fig. 6. Scattered  $V_{\text{full}}$  and  $V_{\text{partial}}$  measured from alpha and beta pulses. The three regions where pulses are classified as either alphas, betas, or based on the CI method are illustrated.

TABLE I  
FOR EVERY POSSIBLE OUTPUT COMBINATION OF THE THREE COMPARATORS "ALPHA COMP", "BETA COMP", AND "CI COMP", THE DEADTIME PRODUCED BY THE CIRCUIT IS INTRODUCED ALONG WITH THE CLASSIFICATION DECISION OF THE CIRCUIT AND THE CASE THAT IS CONSIDERED.

Case	Beta Comp	Alpha Comp	CI Comp	Deadtime [ns]
Beta	0	0	0/1	300
Beta	1	0	0	300
Small Alpha	1	0	1	500
Medium Alpha	1	1	0/1	700
Not Possible	0	1	0/1	-

discriminated by the Alpha comparator. In addition, it can be seen that  $V_{\text{full}}$  of high energy pulses saturate at the power supply of the intergrator, which is about 4.5 V. If the pulses in this region would have been discriminated based on their PSD ratio, they would eventually be miss-classified, but since they are automatically classified as alpha pulses, saturation does not pose any difficulties. Moreover, making use of the Beta comparator and the Alpha comparator extends the dynamic range of the circuit making it suitable for a wider range of incident particles in contrast to solely using the CI comparator. Discrimination of the input pulse is performed by the 3 comparators combined with logic gates and is described in Table I.

### B. Double<sup>+</sup> Counting Rejection

The dedicated D<sup>+</sup>CR block was designed to cope with **Challenge II** and improve neutron counting within high gamma fluxes. More specifically, the D<sup>+</sup>CR block is designed to detect the specific case of two gamma pulses arriving consecutively. This event is both prone to be classified as a neutron and is more likely to occur the higher the gamma flux is.

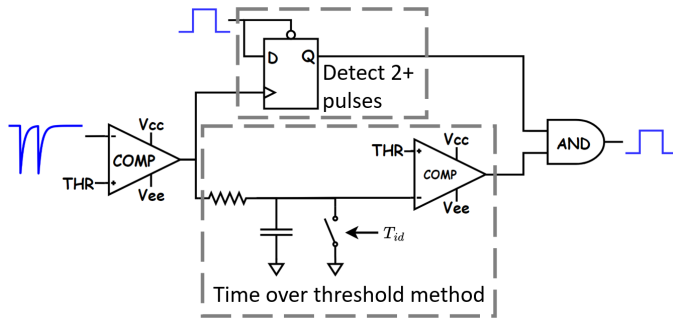


Fig. 7. Illustration of the D<sup>+</sup>CR block.

An illustration of the D<sup>+</sup>CR block can be seen in Fig. 7. The block is fed with the output of the comparator used for detection, which is then fed into two separate channels. The first channel is composed of a D flip-flop (D-FF) which outputs a "high" level whenever two or more pulses are detected. Note that low energy neutrons may produce a pulse that crosses the discrimination level several times, unintentionally triggering a "high" output in this channel. The second channel is composed of an RC network, a SPST switch, and a comparator, which implements a ToT method. The detection comparator output charges the (-) input of the ToT comparator via the RC network. Two consecutive low energy gamma pulses are likely to charge the RC network to a low level, while low energy neutrons are not. A "high" output in both channels causes the D<sup>+</sup>CR block to reject the event. Two examples of signal shapes at different nodes of the D<sup>+</sup>CR block for a low energy alpha pulse and two beta pulses arriving consecutively can be seen in Fig. 8. While the low energy alpha pulse does trigger the D-FF due to the tail re-triggering the detection comparator, the ToT is long enough so that the pulse is not rejected. The two consecutive beta pulses on the other hand both trigger the D-FF and have a low ToT, therefore the output of the D<sup>+</sup>CR goes high and the event is successfully rejected instead of being classified as an alpha.

### C. Dynamic deadtime

In order to cope with **Challenge III**, a varying constant deadtime and a dynamic deadtime is employed. The varying constant deadtimes were introduced in Table I. The DDT block is designed to produce a dynamic deadtime that is proportional to the energy of the arriving pulse. Instead of deploying a simple ToT method which fails to produce a deadtime lasting during afterglow, a method based on peak-detection is deployed. An illustration of the DDT block can be seen in Fig. 9. The pulse from the detector is fed into a high speed amplifier which acts both as an amplifier and as a low-pass filter, capturing the energy deposited. Next, the amplified pulse is fed into an envelope detector. Rising edges of the pulse are immediately passed forward while falling edges aren't, and the output of the envelope detector is discharged using a slow RC network. This way, sharp peaks resulting from afterglow "re-trigger" the deadtime until the slow RC network discharges them.

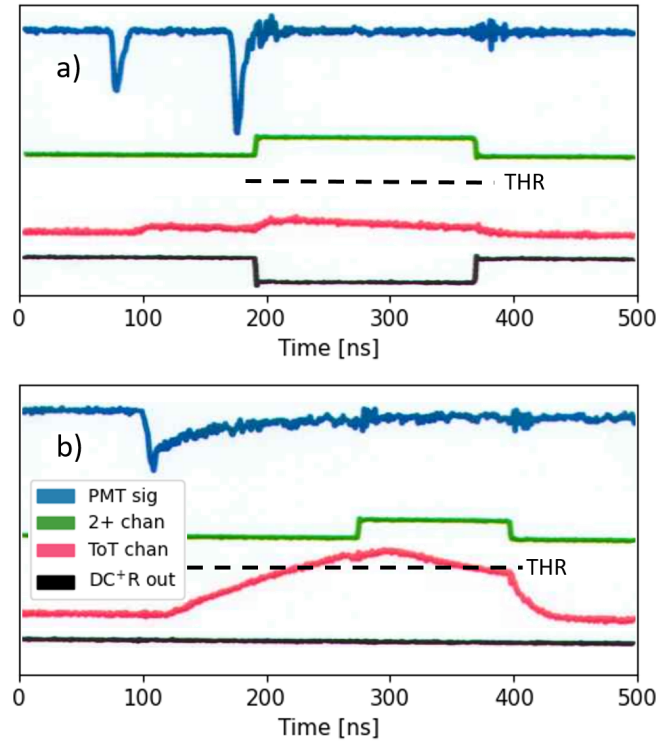


Fig. 8. Signal shape at different nodes of the D<sup>+</sup>CR block (a) for two beta pulses arriving consecutively, (b) for a low energy alpha pulse.

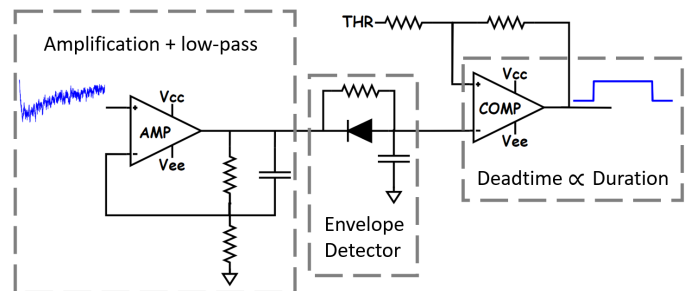


Fig. 9. Illustration of the DDT block.

The detector signal, the amplified signal, and the amplified signal after the envelope detector can be seen in Fig. 10. The detector signal produces an afterglow lasting up to 50  $\mu$ s. Using the ToT method on the detector signal or the amplified signal would unsuccessfully result in a 10  $\mu$ s or a 30  $\mu$ s deadtime, respectively. On the other hand, using the ToT method on the amplified signal after the envelope detector successfully results in a 50  $\mu$ s deadtime, which is proportional to the afterglow produced by the detector signal.

## IV. RESULTS

The topology parameters were adjusted based on the alpha and beta pulse characteristics displayed in section II so that pulses with a decay constant of under 11 ns would be classified as betas, and pulses with decay constants above 11 ns would be classified as alphas.

In order to evaluate the discrimination capabilities of the circuit solely based on the PSD ratio, the following experiment

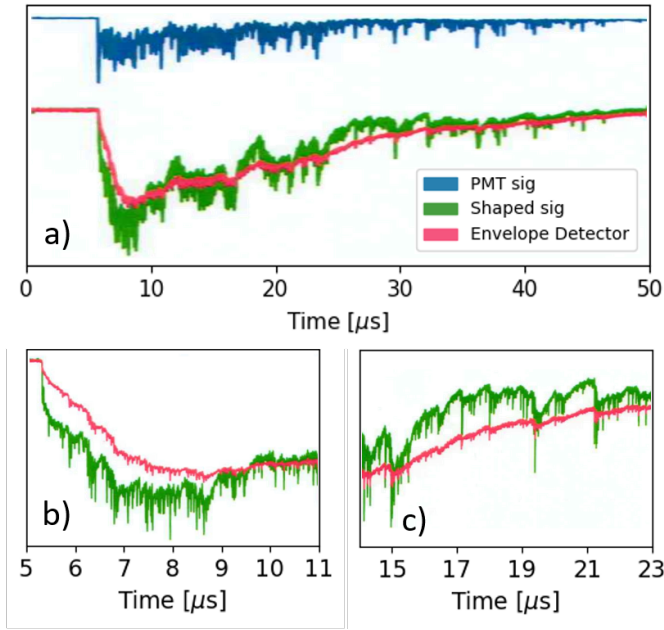


Fig. 10. (a) signal shape at different nodes of the DDT block. (b) Zoomed-in view on the rising edge of the shaped signal, visualizing the envelope detector successfully following the shaped signal. (c) Zoomed-in view on the decaying part of the shaped signal, visualizing the envelope detector signal successfully decaying based on a RC constant, instead of following the shaped signal.

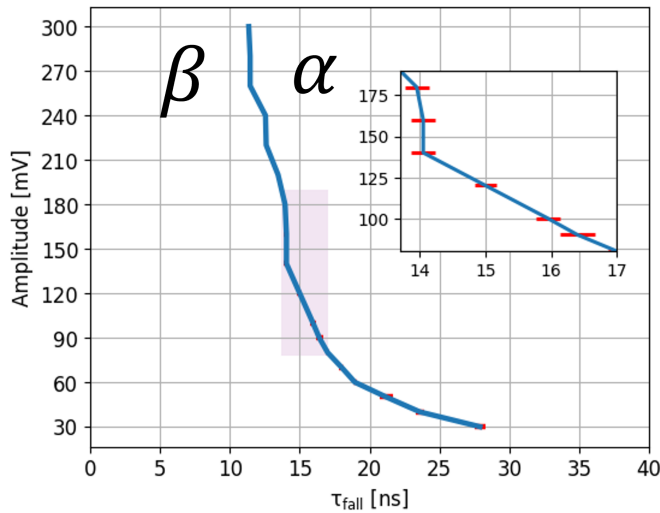


Fig. 11. The decay time programmed in the emulator at which the circuit's discrimination changes for different amplitudes. Error bars are also displayed.

was conducted. Exponential pulses from a fast digital emulator were injected into the circuit at amplitudes ranging between 30 and 300 mV, in 10 mV increments. For each amplitude, the decay constant at which the output of the CI comparator changed its value was found. At least five decay constants near the flipping point were tested in order to evaluate the uncertainty in the flipping region. The results are displayed in Fig. 11.

Firstly, it can be seen in the zoomed-in region highlighted in light purple that the uncertainty in the flipping region is relatively small for all regions, being under 1 ns for all ampli-

tudes above 100 mV. At high amplitudes, the discrimination line is relatively stable around the decay constant of 11 ns. As the amplitude of the pulses goes lower, the discrimination capabilities of the circuit deteriorate and the discrimination line shifts towards higher decay constants. This effect is likely due to a constant charge injection being injected into the integrator capacitor, which introduces the same additive constant to both  $V_{partial}$  and  $V_{full}$ . pulses with smaller amplitudes have smaller  $V_{partial}$  and  $V_{full}$  values, leading to a larger effect from this constant voltage.

A well-established and widely accepted method for quantitative comparison of various PSD techniques is to evaluate the FoM [25]. The method is to fit a double-Gaussian function, in which, each one of the Gaussian functions has a corresponding centroid and a full width at height maximum (FWHM). The FoM is defined in (3).

$$FoM = \frac{|\mu_n - \mu_g|}{FWHM_n + FWHM_g} \quad (3)$$

In order to evaluate the discrimination capabilities of the circuit on the detector introduced in section II, the output of the partial integrator and the full integrator were recorded for 20,000 alpha pulses and 20,000 beta pulses from the experiment detailed in section II. The PSD ratio was then calculated using sampled  $V_{partial}$  and  $V_{full}$  values. Fig. 12 displays a histogram of the PSD ratios obtained, with a calculated FoM of 2.35.

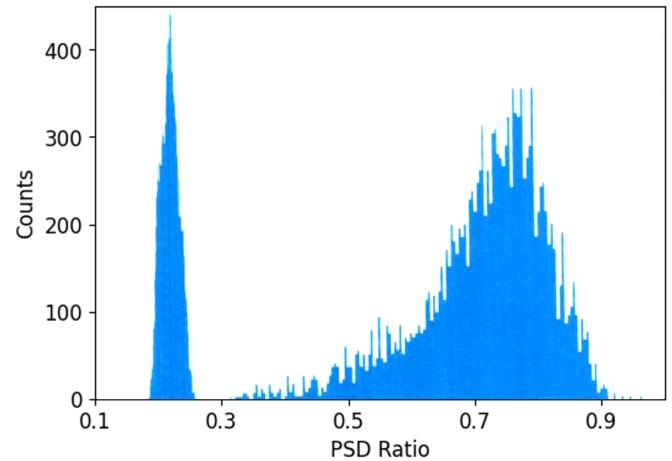


Fig. 12. Histogram of the PSD ratio measured for the 20,000 alpha pulses and 20,000 beta pulses discriminated by the circuit.

In order to evaluate the discrimination capabilities at different amplitudes the FoM was calculated for several amplitude bins. The FoM calculated at 10 equally spaced points between 20 mV and 200 mV are displayed in Fig. 13. At each of these points  $A_i$ , the FoM was calculated using pulses with amplitudes lying in the interval  $A_i \pm 10$  mV. As expected, it can be seen that the FoM improves as the amplitude of the pulses, which is proportional to the SNR, increases.

The goal of the  $D^+CR$  block is to reject cases where two gamma pulses arrive consecutively in order to reduce neutron miss-classifications. The effectiveness of the  $D^+CR$  was tested

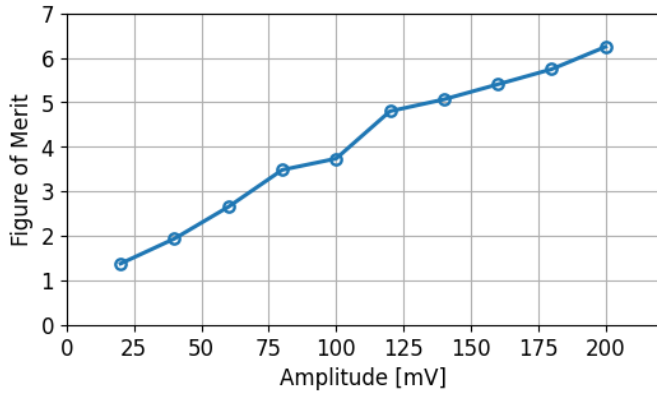


Fig. 13. The FoM calculated from the PSD ratios displayed in Fig. 12 at several amplitude ranges. The amplitude range corresponding to each amplitude point  $A_i$  displayed is  $A_i \pm 10$  mV.

using the fast digital emulator. The emulator was set to produce beta signals with the arrival process resembling a Poisson point process, and the number of pulses classified by the circuit as alphas were counted for beta fluxes ranging between 1 kcps and 100 kcps. Ideally, the desired output would be no alpha classifications for all event rates, but due to **Challenge II** as the beta flux increases so does the number of false alpha detections. The results obtained both when the  $D^+CR$  block was connected and disconnected can be seen in Fig. 14.

It can be seen that for all beta fluxes the  $D^+CR$  block successfully lowers the number of false alpha detections by a factor of up to 4. The remaining miss-classifications result from either the occurrence of three or more beta pulses within a single integration window, or the presence of two closely spaced beta pulses that cannot be rejected by the  $D^+CR$  block.

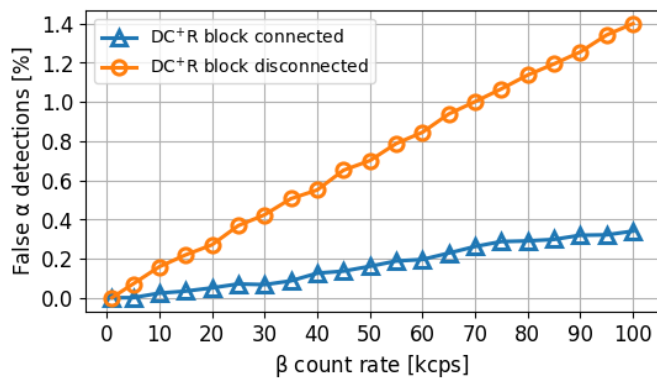


Fig. 14. The percentage of false  $\alpha$  detections for different beta fluxes with the  $D^+CR$  block connected and disconnected.

The effectiveness of the DDT block can be seen in Fig. 10, where the produced signal successfully creates a deadtime proportional to the length of the afterglow produced by the initial pulse. The fast digital emulator was used in order to validate the expected behavior of the block, where higher energy pulses are required to produce longer deadtimes. Pulses with varying total charge were injected into the circuit and the resulting deadtime was measured. The results can be seen in Fig. 15. Pulses with total charge which is not high enough to trigger

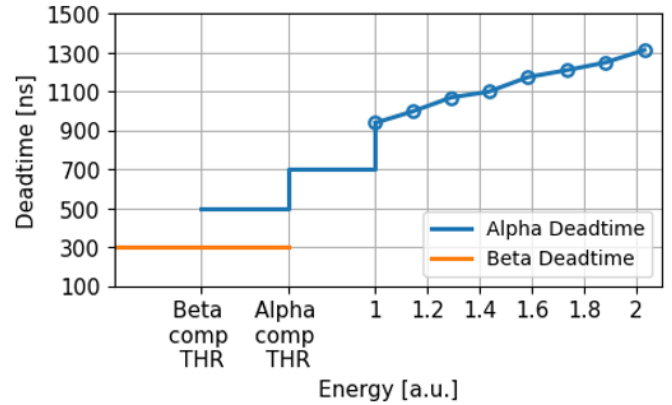


Fig. 15. The measured deadtime produced by the circuit as a function of both the charge of the arriving nuclear pulse and the discrimination made by the circuit.

the DDT block yield varying constant deadtimes which are detailed in Table I. For higher energy alpha pulses, the DDT block successfully produces a deadtime that is proportional to the energy of the alpha pulse. By successfully producing a deadtime proportional to the energy of the alpha pulses, the circuit is ensured to have a smaller overall deadtime, which yields more pulse detections in total.

## V. CONCLUSION

A novel analog PSD topology based on the well-known CI method designed for fast scintillators has been developed and implemented on an FR-4 PCB. A FoM of 2.35 was calculated for alpha and beta pulses from a plastic scintillator with a ZnS(Ag) layer coupled to a PMT. The topology has a dedicated block designed to reject fast pulses arriving consecutively, resulting in up to four times less slow pulse miss-classifications in fast pulse event rates ranging up to 100 kcps. Moreover, the dedicated block that yields a dynamic deadtime proportional to the energy of the pulse is proved to be beneficial for lowering the total deadtime and improving detection efficiency. The topology does not require fast ADCs, therefore it may be suitable for low power applications. The topology is versatile and can easily be adapted for different detectors with different pulse shapes by adjusting several passive electronic components.

## REFERENCES

- [1] A. Dutta and K. E. Holbert, "Discrimination of neutron-gamma ray pulses with pileup using normalized cross correlation and principal component analysis," *IEEE Transactions on Nuclear Science*, vol. 63, no. 6, pp. 2764–2771, 2016.
- [2] C. Fu, A. Di Fulvio, S. Clarke, D. Wentzloff, S. Pozzi, and H. Kim, "Artificial neural network algorithms for pulse shape discrimination and recovery of piled-up pulses in organic scintillators," *Annals of nuclear energy*, vol. 120, pp. 410–421, 2018.
- [3] A. Dutta, P. Chandhran, K. E. Holbert, and E. B. Johnson, "Using decay time to discriminate neutron and gamma ray pulses from a clyc detector," in *2015 IEEE Nuclear Science Symposium and Medical Imaging Conference (NSS/MIC)*. IEEE, 2015, pp. 1–7.
- [4] S. Richards, G. Sykora, and M. Taggart, "High count rate pulse shape discrimination algorithms for neutron scattering facilities," *Nuclear Instruments and Methods in Physics Research Section A: Accelerators, Spectrometers, Detectors and Associated Equipment*, vol. 989, p. 164946, 2021.

- [5] J. Polack, M. Flaska, A. Enqvist, C. Sosa, C. Lawrence, and S. Pozzi, "An algorithm for charge-integration, pulse-shape discrimination and estimation of neutron/photon misclassification in organic scintillators," *Nuclear Instruments and Methods in Physics Research Section A: Accelerators, Spectrometers, Detectors and Associated Equipment*, vol. 795, pp. 253–267, 2015.
- [6] M. Nakhostin, "A general-purpose digital pulse shape discrimination algorithm," *IEEE Transactions on Nuclear Science*, vol. 66, no. 5, pp. 838–845, 2019.
- [7] R. M. French, M. Thevenin, M. Hamel, and E. Montbarbon, "A histogram-difference method for neutron/gamma discrimination using liquid and plastic scintillators," *IEEE Transactions on Nuclear Science*, vol. 64, no. 8, pp. 2423–2432, 2017.
- [8] M. Safari, F. A. Davani, H. Afarideh, S. Jamili, and E. Bayat, "Discrete fourier transform method for discrimination of digital scintillation pulses in mixed neutron-gamma fields," *IEEE transactions on nuclear science*, vol. 63, no. 1, pp. 325–332, 2016.
- [9] H. Singh and R. Mehra, "Discrete wavelet transform method for high flux  $n - \gamma$  discrimination with liquid scintillators," *IEEE Transactions on Nuclear Science*, vol. 64, no. 7, pp. 1927–1933, 2017.
- [10] M. Hammad, H. Kasban, R. Fikry, M. I. Dessouky, O. Zahran, S. M. Elaraby, and F. E. A. El-Samie, "Digital pulse processing algorithm for neutron and gamma rays discrimination," *Analog Integrated Circuits and Signal Processing*, vol. 101, pp. 475–487, 2019.
- [11] B. Blair, C. Chen, A. Glenn, A. Kaplan, J. Ruz, L. Simms, and R. Wurtz, "Gaussian mixture models as automated particle classifiers for fast neutron detectors," *Statistical Analysis and Data Mining: The ASA Data Science Journal*, vol. 12, no. 6, pp. 479–488, 2019.
- [12] A. Glenn, Q. Cheng, A. D. Kaplan, and R. Wurtz, "Pulse pileup rejection methods using a two-component gaussian mixture model for fast neutron detection with pulse shape discriminating scintillator," *Nuclear Instruments and Methods in Physics Research Section A: Accelerators, Spectrometers, Detectors and Associated Equipment*, vol. 988, p. 164905, 2021.
- [13] M. Gelfusa, R. Rossi, M. Lungaroni, F. Belli, L. Spolladore, I. Wyss, P. Gaudio, A. Murari, and J. Contributors, "Advanced pulse shape discrimination via machine learning for applications in thermonuclear fusion," *Nuclear Instruments and Methods in Physics Research Section A: Accelerators, Spectrometers, Detectors and Associated Equipment*, vol. 974, p. 164198, 2020.
- [14] E. Doucet, T. Brown, P. Chowdhury, C. Lister, C. Morse, P. Bender, and A. Rogers, "Machine learning  $n/\gamma$  discrimination in clyc scintillators," *Nuclear Instruments and Methods in Physics Research Section A: Accelerators, Spectrometers, Detectors and Associated Equipment*, vol. 954, p. 161201, 2020.
- [15] T. Tambouratzis, D. Chernikova, and I. Pzsis, "Pulse shape discrimination of neutrons and gamma rays using kohonen artificial neural networks," *Journal of Artificial Intelligence and Soft Computing Research*, vol. 3, no. 2, pp. 77–88, 2013.
- [16] J. Griffiths, S. Kleinegessse, D. Saunders, R. Taylor, and A. Vacheret, "Pulse shape discrimination and exploration of scintillation signals using convolutional neural networks," *Machine Learning: Science and Technology*, vol. 1, no. 4, p. 045022, 2020.
- [17] M. Astrain, M. Ruiz, A. V. Stephen, R. Sarwar, A. Carpeño, S. Esquem-bri, A. Murari, F. Belli, and M. Riva, "Real-time implementation of the neutron/gamma discrimination in an fpga-based daq mtca platform using a convolutional neural network," *IEEE Transactions on Nuclear Science*, vol. 68, no. 8, pp. 2173–2178, 2021.
- [18] X. Fabian, G. Baulieu, L. Ducroux, O. Stézowski, A. Boujrad, E. Clément, S. Coudert, G. de France, N. Erduran, S. Ertürk *et al.*, "Artificial neural networks for neutron/ $\gamma$  discrimination in the neutron detectors of neda," *Nuclear Instruments and Methods in Physics Research Section A: Accelerators, Spectrometers, Detectors and Associated Equipment*, vol. 986, p. 164750, 2021.
- [19] J. Han, J. Zhu, Z. Wang, G. Qu, X. Liu, W. Lin, Z. Xu, Y. Huang, M. Yan, X. Zhang *et al.*, "Pulse characteristics of clyc and piled-up neutron-gamma discrimination using a convolutional neural network," *Nuclear Instruments and Methods in Physics Research Section A: Accelerators, Spectrometers, Detectors and Associated Equipment*, vol. 1028, p. 166328, 2022.
- [20] S. Peng, Z. Hua, Q. Wu, J. Han, S. Qian, Z. Wang, Q. Wei, L. Qin, L. Ma, M. Yan *et al.*, "Piled-up neutron-gamma discrimination system for cllb using convolutional neural network," *Journal of Instrumentation*, vol. 17, no. 08, p. T08001, 2022.
- [21] M. Flaska and S. A. Pozzi, "Identification of shielded neutron sources with the liquid scintillator bc-501a using a digital pulse shape discrimination method," *Nuclear Instruments and Methods in Physics Research Section A: Accelerators, Spectrometers, Detectors and Associated Equipment*, vol. 577, no. 3, pp. 654–663, 2007.
- [22] M. Nakhostin and P. Walker, "Application of digital zero-crossing technique for neutron-gamma discrimination in liquid organic scintillation detectors," *Nuclear Instruments and Methods in Physics Research Section A: Accelerators, Spectrometers, Detectors and Associated Equipment*, vol. 621, no. 1-3, pp. 498–501, 2010.
- [23] D. Cester, M. Lunardon, G. Nebbia, L. Stevanato, G. Viesti, S. Petrucci, and C. Tintori, "Pulse shape discrimination with fast digitizers," *Nuclear Instruments and Methods in Physics Research Section A: Accelerators, Spectrometers, Detectors and Associated Equipment*, vol. 748, pp. 33–38, 2014.
- [24] G. J. Sykora, E. M. Schooneveld, and N. J. Rhodes, "Zno: Zn/6lif scintillator—a low afterglow alternative to zns: Ag/6lif for thermal neutron detection," *Nuclear Instruments and Methods in Physics Research Section A: Accelerators, Spectrometers, Detectors and Associated Equipment*, vol. 883, pp. 75–82, 2018.
- [25] M. J. Balmer, K. A. Gamage, and G. C. Taylor, "Comparative analysis of pulse shape discrimination methods in a 6li loaded plastic scintillator," *Nuclear Instruments and Methods in Physics Research Section A: Accelerators, Spectrometers, Detectors and Associated Equipment*, vol. 788, pp. 146–153, 2015.